



Zinc *K*-edge XANES spectroscopy of mineral and organic standards

Erin Castorina,^a Ellery D. Ingall,^{a*} Peter L. Morton,^b David A. Tavakoli^c and Barry Lai^d

^aSchool of Earth and Atmospheric Sciences, Georgia Institute of Technology, 311 Ferst Dr NW, Atlanta, GA 30332-0340, USA, ^bGeochemistry, National High Magnetic Field Laboratory, 1800 E Paul Dirac Dr, Tallahassee, FL 32310, USA, ^cMaterials Characterization Facility, Georgia Institute of Technology, 345 Ferst Dr NW, Atlanta, GA 30332-1000, USA, and ^dAdvanced Photon Source, Argonne National Laboratory, 9700 South Cass Avenue, Argonne, IL 60439, USA.

*Correspondence e-mail: ellery.ingall@eas.gatech.edu

Received 24 January 2019

Accepted 19 April 2019

Edited by R. W. Strange, University of Essex, UK

Keywords: zinc standards; Zn *K*-edge; XANES; spectroscopy.

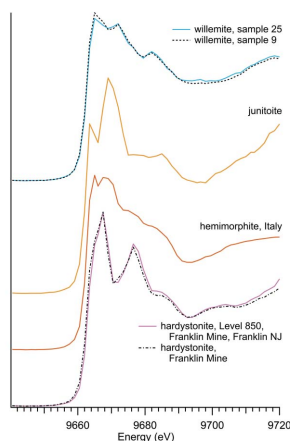
Supporting information: this article has supporting information at journals.iucr.org/s

Zinc *K*-edge X-ray absorption near-edge (XANES) spectroscopy was conducted on 40 zinc mineral samples and organic compounds. The *K*-edge position varied from 9660.5 to 9666.0 eV and a variety of distinctive peaks at higher post-edge energies were exhibited by the materials. Zinc is in the +2 oxidation state in all analyzed materials, thus the variations in edge position and post-edge features reflect changes in zinc coordination. For some minerals, multiple specimens from different localities as well as pure forms from chemical supply companies were examined. These specimens had nearly identical *K*-edge and post-edge peak positions with only minor variation in the intensity of the post-edge peaks. This suggests that typical compositional variations in natural materials do not strongly affect spectral characteristics. Organic zinc compounds also exhibited a range of edge positions and post-edge features; however, organic compounds with similar zinc coordination structures had nearly identical spectra. Zinc XANES spectral patterns will allow identification of unknown zinc-containing minerals and organic phases in future studies.

1. Introduction

Zinc *K*-edge X-ray absorption near-edge spectroscopy (XANES) is a valuable tool for determining the solid-phase chemical speciation of zinc across a wide range of disciplines and applications. Agriculturally, research includes using zinc to enhance the grain concentration of plants (Doolette *et al.*, 2018) and using colloidal particles to increase the rate of discharge of zinc and phosphorus from swine manure used as a fertilizer (Yamamoto & Hashimoto, 2017). Industrial studies have looked at the speciation of zinc in a fly ash spill (Rivera *et al.*, 2017) and steelmaking sludge (Wang *et al.*, 2013). Environmentally, there has been research into heavy metals in combined sewer overflow discharge (Rouff *et al.*, 2013) and organic waste amended soil as fertilizer (Tella *et al.*, 2016; Mamindy-Pajany *et al.*, 2014). Because XANES measures structural composition, other research has included multiple nanotechnology studies (Zhou *et al.*, 2017; Frenkel *et al.*, 2001). However, research is not limited to environmental and industrial applications, as zinc *K*-edge XANES has also been used to analyze the paint in historic paintings, without degrading the pigments (Gervais *et al.*, 2015).

Zinc, as a bioactive trace metal, is a vital nutrient for all living organisms, yet can also be toxic at high concentrations. The chemical form of zinc can be a key factor in determining its potential bioavailability or toxicity to organisms. In turn, zinc bioavailability has implications for the health and



productivity of riverine (Le Pape *et al.*, 2014), terrestrial (Isaure *et al.*, 2005; Webb & Gaillard, 2015; Manceau *et al.*, 2002; Sarret *et al.*, 2004) and marine systems (Löscher, 1999). In marine environments, zinc is a component of two enzymes – carbonic anhydrase and alkaline phosphatase (Sunda & Huntsman, 2005). These enzymes are critical for the growth of most planktonic organisms serving as primary producers at the base of the food chain. In marine diatoms, which account for 20% of total global primary productivity (Malviya *et al.*, 2016), zinc is vital in the growth of their hard silica exoskeleton (Ellwood & Hunter, 2000).

A common approach in the study of elemental cycling within natural systems is to fit XANES spectra of unknown samples with spectra of known, well characterized materials (Leinweber *et al.*, 2007; Gaur *et al.*, 2009; Gräfe *et al.*, 2014; Da Silva-Cadoux *et al.*, 2012; Oakes *et al.*, 2012; Longo *et al.*, 2014). For many elemental systems, including zinc, comprehensive databases of XANES spectra are not available, which makes it more difficult to interpret spectra of unknown materials. Although plots of Zn-XANES spectra for standards of a limited number of materials may appear in studies, such as the ones listed above, the data for these spectra is typically not provided. Some previous zinc spectroscopy studies focused on standards created for EXAFS at a temperature of 20 K (Jacquat *et al.*, 2009), but a large, comprehensive set of zinc *K*-edge XANES, which would be especially relevant for measurements under environmental conditions (Monsant *et al.*, 2011), does not appear to currently exist.

The breadth of zinc standards that can be analyzed concurrently with the research being conducted is often limited by scheduling constraints. As a result, many studies must rely on a small sample set of zinc standards which is then used to inform the XANES analysis of the focus of the research (Cheng *et al.*, 2018; Wang *et al.*, 2007; Dessombz *et al.*, 2013; Adediran *et al.*, 2015). The zinc standard references presented here (Table S1 of the supporting information) will provide researchers with a diverse spectra database to initiate studies of zinc mineral speciation, thereby saving valuable synchrotron time for sample analyses. These references include both natural and synthetic materials, which will be useful in characterizing the mineral speciation of zinc in natural and anthropogenically impacted settings.

2. Methods

Zinc spectroscopy was run on 34 different mineral or inorganic phases and six zinc-containing organic phases. Multiple samples of some of the naturally occurring minerals were measured to evaluate the effects of compositional variations within one mineral species. The samples were either in private collections or were obtained from mineral dealers or chemical supply companies. The identity of all minerals, with the exception of one hetaerolite sample with insufficient sample mass, was verified with powder X-ray diffraction (XRD) at the Georgia Institute of Technology.

The zinc materials were measured at the 2-ID-D beamline at the Advanced Photon Source synchrotron at Argonne

National Laboratories in Illinois, USA. This beamline has an energy range of 5–30 keV and a focused flux of 4×10^9 photons s^{-1} at 10 keV which makes it ideal for high-resolution X-ray imaging (Ingall *et al.*, 2018). The source of the beamline is a 3.3 cm-period undulator, and a Kohzu Si (111) monochromator was used to provide an energy resolution of $1.4 \times 10^{-4} \Delta E/E$. The energy was calibrated at 9659 eV using the inflection point of the *K*-edge of a zinc metal foil standard material. The samples were ground to a fine powder ($<10 \mu\text{m}$) to minimize self-absorption. Comparing the fluorescence with the transmission data confirms that the samples were sufficiently thin to avoid self-absorption in accordance with previously accepted methods (Waychunas *et al.*, 2003). Less than 1 mg of powder was distributed over approximately 1 cm^2 of cellulose acetate membrane which was then placed over a slot on an aluminium mounting stick. For these experiments, the undulator was tuned to 9.68 keV and the energy scan was conducted in 0.5 eV steps between 9.64 and 9.72 keV while the X-ray fluorescence signal was collected by a silicon drift detector (Vortex-EM).

Using the fluorescence signal, the Zn-NEXFS (zinc near-edge X-ray fluorescence spectroscopy) data were collected. Zn-NEXFS differs from Zn-XANES in the signal detection, in that it uses the fluorescence signal to obtain an absorption signal which is inversely proportional to the XANES signal. The fluorescence detector only measures the signal from the interactions of the beam with the zinc atoms. In contrast, in the ion chamber used for XANES measurements an extremely small percentage of the incoming radiation reaching the ion chamber is absorbed by Zn atoms. Thus the absorption signal is extremely small relative to the large amount of radiation reaching the detector. Use of the fluorescence detector allows for a signal with minimal background. This is undoubtedly why fluorescence is the method most frequently employed for natural samples. The samples were analyzed three to five times with a dwell time ranging from 0.5 to 3 s per step, with higher dwell times given to samples with low concentrations. Care was taken to minimize detector saturation and the dead time ($<10\%$), while optimizing the signal, by adjusting the detector position and the size of the slits, in accordance with methods to optimize the quality of analysis conducted using fluorescence in X-ray absorption spectroscopy (XAS) analysis as discussed in the literature (Abe *et al.*, 2018; Gräfe *et al.*, 2014; Waychunas *et al.*, 2003).

The spectra were analyzed with *ATHENA* XAS data processing software (*Demeter* 0.9.26 using *Ifeffit* 1.2.12) (Ravel & Newville, 2005). The X-ray fluorescence signal was normalized by dividing the zinc counts by the upstream ion chamber counts. Since each sample had been scanned multiple times, these scans were aligned within *ATHENA* based on the smoothed derivative of energy before merging the absorption edge, with importance placed on larger edge steps, in order to assign higher importance to spectra obtained from a more concentrated sample. Edge-step positions were determined by using the first derivative of the spectra.

All XANES data is provided in Table S1 of the supporting information.

The identity of the mineral samples was verified on a Malvern PANalytical Empyrean multi-technique X-ray diffractometer and a copper radiation source. Data analysis was conducted with the *HighScore Plus* software associated with the diffractometer, and a third-party database, PDF 4+, from the International Centre for Diffraction Data (ICDD). Each sample was approximately a gram in size and was placed on a silica zero plate to minimize background signals from the sample mount. The masks and slits on the Empyrean X-ray diffractometer were set for the small sample size and each mineral was analyzed for 10–40 s per step, with a 2Θ range from 10–90°. Many of the samples were analyzed while spinning at 3.755 rpm, to minimize diffraction errors. XRD data are provided in the supporting information.

3. Results and discussion

The XANES spectra of all zinc materials in this study had principal *K*-edge peak energies between 9660.5 and 9666.0 eV. This peak results from the excitation of an electron from a 1s inner orbital to higher-energy orbitals as a result of interaction with a synchrotron-generated X-ray. Subsequent decay of higher-energy electrons to unoccupied 1s orbitals releases photons, which are counted by the Vortex-EM detector. The minerals and organics measured in this study contained zinc in the +II oxidation state. Although the structural position of

Table 1
Zinc silicates.

Sample number	Name	Ideal chemical formula	Locality	E_0 (eV)
32	Hardystonite	$\text{Ca}_2\text{Zn}(\text{Si}_2\text{O}_7)$	850 Level, Hamburg Mine, Franklin, NJ, USA	9663.5
40	Hardystonite	$\text{Ca}_2\text{Zn}(\text{Si}_2\text{O}_7)$	Franklin, NJ, USA	9663.5
4	Hemimorphite	$\text{Zn}_4\text{Si}_2\text{O}_7(\text{OH})_2 \cdot \text{H}_2\text{O}$	Private collection, unknown locality	9663.5
6	Hemimorphite	$\text{Zn}_4\text{Si}_2\text{O}_7(\text{OH})_2 \cdot \text{H}_2\text{O}$	Private collection, unknown locality	9663.5
24	Hemimorphite	$\text{Zn}_4\text{Si}_2\text{O}_7(\text{OH})_2 \cdot \text{H}_2\text{O}$	Private collection, unknown locality	9663.5
36	Hemimorphite	$\text{Zn}_4\text{Si}_2\text{O}_7(\text{OH})_2 \cdot \text{H}_2\text{O}$	79 Mine, Banner District, Gila Co., AZ, USA	9663.5
37	Hemimorphite	$\text{Zn}_4\text{Si}_2\text{O}_7(\text{OH})_2 \cdot \text{H}_2\text{O}$	Sardinia, Italy	9663.5
31	Junitoite	$\text{CaZn}_2\text{Si}_2\text{O}_7 \cdot \text{H}_2\text{O}$	Christmas Mine, Gila County, AZ, USA	9663.5
25	Willemite	Zn_2SiO_4	Private collection, unknown locality	9663.5
9	Willemite	Zn_2SiO_4	Private collection, unknown locality	9663.5

zinc within the mineral lattice would be expected to exert a major influence on spectral features, a study investigating the impact of tetrahedral versus octahedral coordination on spectral features shows that these changes are subtle (Waychunas *et al.*, 2003).

Spectra of most minerals also revealed additional pre-edge or post-edge features that can be used to identify specific minerals or differentiate between mineral groups. In general, these pre- and post-edge features are related to (i) the presence and weight percent of different elements; (ii) the oxidation state of these elements; and (iii) the arrangement of these elements in the mineral structure. More information on pre-edge and post-edge features for specific minerals and mineral groups follows.

3.1. Zinc silicates

Four unique zinc silicate minerals were studied including three sorosilicates – hardystonite, hemimorphite and junitoite – and one nesosilicate – willemite (Table 1), with spectra shown in Fig. 1. The analysis includes five separate samples of the zinc silicate hemimorphite (Fig. 2), to assess spectroscopic

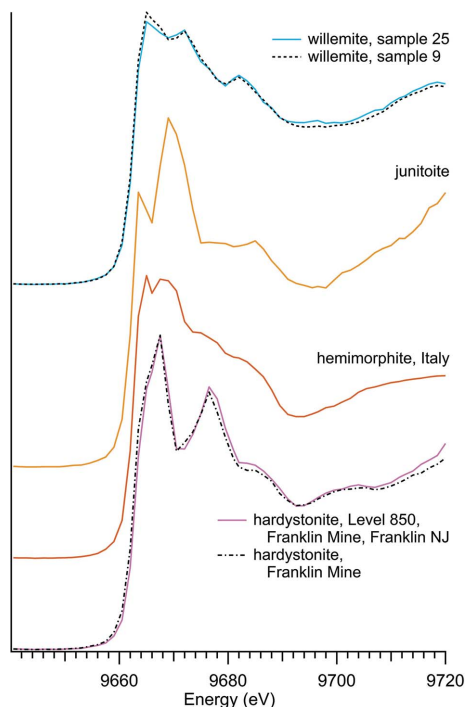


Figure 1
Zinc silicate spectra.

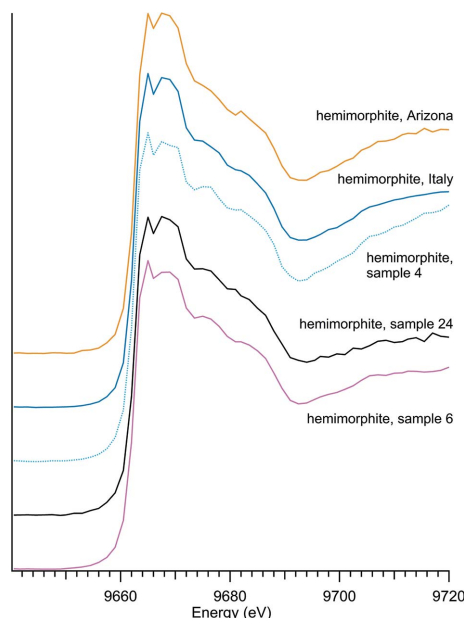


Figure 2
Comparison of hemimorphite minerals.

Table 2
Zinc carbonates.

Sample number	Name	Ideal chemical formula	Locality	E_0 (eV)
41	Hydrozincite	$Zn_5(CO_3)_2(OH)_6$	Goodsprings, NV, USA	9663.5
35	Rosasite	$(Cu,Zn)_2(CO_3)(OH)_2$	Kelly Mine, Magdalena, NM, USA	9663.5
26	Smithsonite	$ZnCO_3$	Private collection, unknown location	9666.0
N/A	Zinc carbonate	$Zn_5(CO_3)_2 \cdot (OH)_6$	Alfa A14590	9663.5

Table 3
Zinc phosphates.

Sample number	Name	Ideal chemical formula	Locality	E_0 (eV)
5	Scholzite	$CaZn_2(PO_4)_2 \cdot 2H_2O$	Private collection, unknown location	9663.5
8	Tarbuttite	$Zn_2(PO_4)(OH)$	Zambia Broken Hill Mine	9663.5
17	Zinc phosphate hydrate	$Zn_3(PO_4)xH_2O$	Alfa 11589	9663.5

variation across natural samples from different locations. The absorption edge position of 9663.5 eV was the same for all zinc silicates regardless of composition. Zinc silicate spectra all have two distinctive peaks at post-edge energies, the strength of which appears to be unique to this mineral class. Sorosilicate versus nesosilicate arrangement of the Si tetrahedrons does not appear to be the primary control of spectral features as the three sorosilicates each have post-edge peaks at different energies (junitoite at 9669 eV, hardystonite at 9676 eV and a broad hemimorphite secondary peak around 9668 eV).

3.2. Zinc carbonates

Three natural zinc carbonate minerals – hydrozincite, rosasite and smithsonite – were observed alongside a commercial basic zinc carbonate (Table 2) with spectra shown

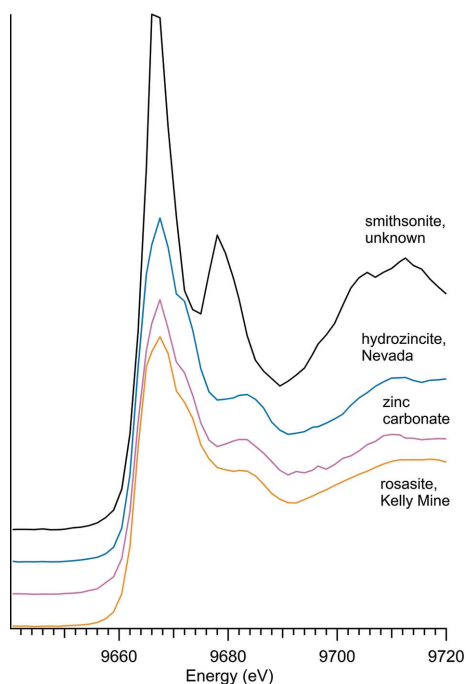


Figure 3
Zinc carbonate spectra.

in Fig. 3. The edge positions for the hydrous forms – hydrozincite, rosasite and basic zinc carbonate – are all at 9663.5 eV, and the anhydrous smithsonite edge is at 9666.0 eV. The spectra of the hydrous zinc carbonates are all characterized by a wider main peak with a prominent shoulder and a higher-energy peak at approximately 9681 eV. Smithsonite differs from the hydrous zinc carbonates with a narrower main peak without a prominent shoulder, a very strong higher-energy peak at 9678 eV, and a wider peak around 9710 eV. These results match well with previous analysis of smithsonite,

including those measured in transmission mode (Gao *et al.*, 2014) and in fluorescence mode (Bazin *et al.*, 2009).

3.3. Zinc phosphates

Zinc phosphates are distinguishable from the larger selection of oxyanions because of the similarity of their spectra (Fig. 4) and the consistency of the initial *K*-edge peak energy of 9663.5 eV (Table 3). The zinc phosphates contained within this study are the natural minerals scholzite and tarbuttite and a synthetic zinc phosphate hydrate. Zinc phosphate spectra are characterized by a wide main peak which is likely due to the presence of a higher-energy peak at 9670 eV. All of the zinc phosphate spectra have a secondary peak at approxi-

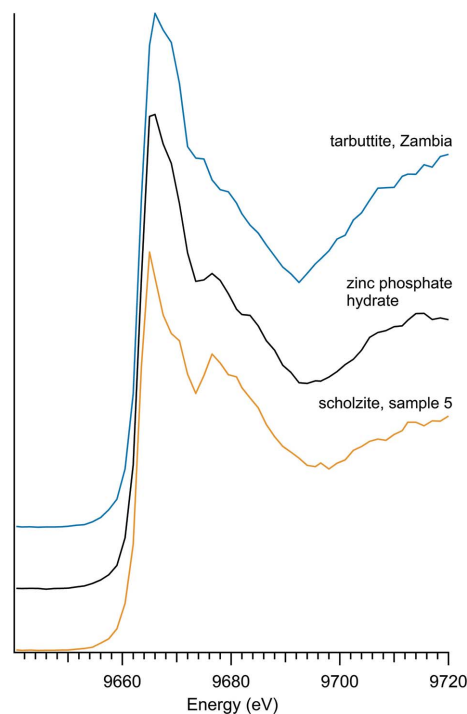


Figure 4
Zinc phosphate spectra.

Table 4
Additional zinc oxyanions.

Sample number	Name	Ideal chemical formula	Locality	E_0 (eV)
30	Adamite	$Zn_2(AsO_4)(OH)$	Mina Ojuela, Mapimi, Durango, Mexico	9663.5
39	Adamite	$Zn_2(AsO_4)(OH)$	Chihuahua, Mexico	9663.5
1	Ammonium zinc sulfate hydrate	$(NH_4)_2Zn(SO_4)_2 \cdot H_2O$	Alfa A13584	9665.0
29	Descloizite	$PbZn(VO_4)(OH)$	Berg Aukas Mine, Grootfontein District, Namibia	9666.0
28	Legrandite	$Zn_2(AsO_4)(OH) \cdot H_2O$	Mina Ojuela, Mapimi, Durango, Mexico	9663.5
15	Zinc nitrate hexahydrate	$Zn(NO_3)_2 \cdot 6H_2O$	Acros Organics 211660050	9663.5
19	Zinc sulfate heptahydrate	$(SO_4)Zn \cdot 7H_2O$	Alfa 33399	9665.0

mately 9676.5 eV which varies in intensity in the different zinc phosphates.

3.4. Other zinc minerals and compounds with zinc oxyanions

Zinc compounds with oxyanions other than phosphate were investigated (Table 4), with spectra shown in Fig. 5. Zinc arsenates are shown separately in Fig. 6 to further illustrate the reproducibility of XANES spectra, regardless of sample location. The zinc arsenates have a nearly identical edge shape and intensity, with divergence only occurring post-edge, around 9680 eV.

3.5. Zinc oxides

There were four zinc oxide materials used in this study: three naturally occurring minerals – franklinite, gahnite and hetaerolite – and a synthetic zinc oxide compound (Table 5 and Fig. 7).

The spectra for the naturally occurring minerals do not resemble the spectra for zinc oxide. Franklinite more closely

matches the spectra for hardystonite and willemite, minerals with which franklinite is closely associated in natural environments. A comparison of these spectra is shown in Fig. 8. Although franklinite, dominated by three strong peaks, appears aberrant, it matches well with previously run franklinite Zn *K*-edge spectra (Waychunas *et al.*, 2003; Hamilton *et al.*, 2016).

There were two samples of hetaerolite, but due to the difficulty of extraction of this mineral there was not enough of the sample from Mohawk Mine to allow for independent verification using the X-ray diffractometer. However, given the similarities of the XAS spectra, and the identical *K*-edge energy, there is a high level of confidence in the identification of the hetaerolite sample from Mohawk Mine.

The zinc oxide sample had one of the lowest observed *K*-edge values. However, the unique shape and low energy level of the zinc *K*-edge may have implications for positively identifying anthropogenic zinc oxides using XANES (Hamilton *et al.*, 2016).

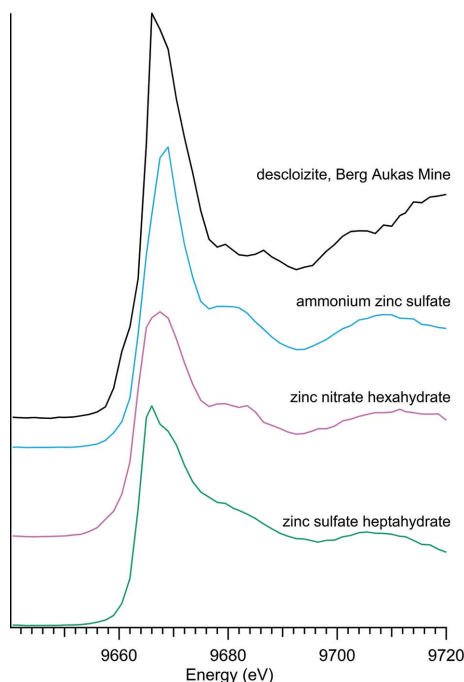


Figure 5
Zinc oxyanion spectra.

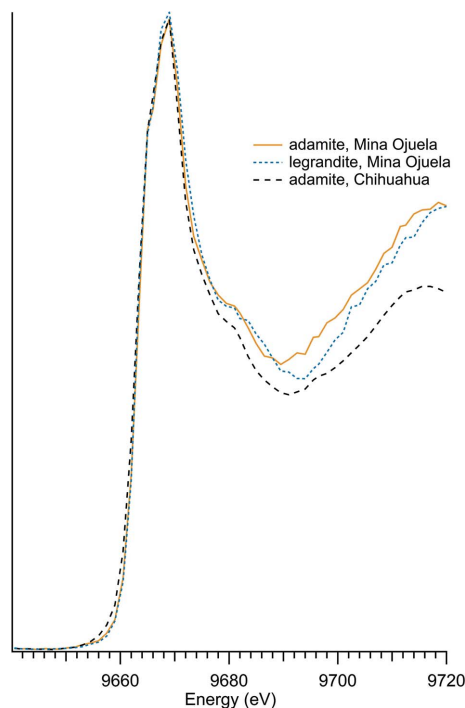


Figure 6
Zinc arsenate spectra.

Table 5
Zinc oxides.

Sample number	Name	Ideal chemical formula	Locality	E_0 (eV)
22	Franklinite	ZnFe ₂ O ₄	Franklin, NJ, USA, private collection of Ellery Ingall	9663.5
33	Gahnite	ZnAl ₂ O ₄	Falun Mine, Falun, Dalarna, Sweden	9663.5
34	Hetaerolite	ZnMn ₂ O ₄	Mohawk Mine, San Bernardino County, CA, USA	9665.0
38	Hetaerolite	ZnMn ₂ O ₄	Carnahan Mine, Golden, NM, USA	9665.0
16	Zinc oxide	ZnO	CAS 1314-13-2	9662.0

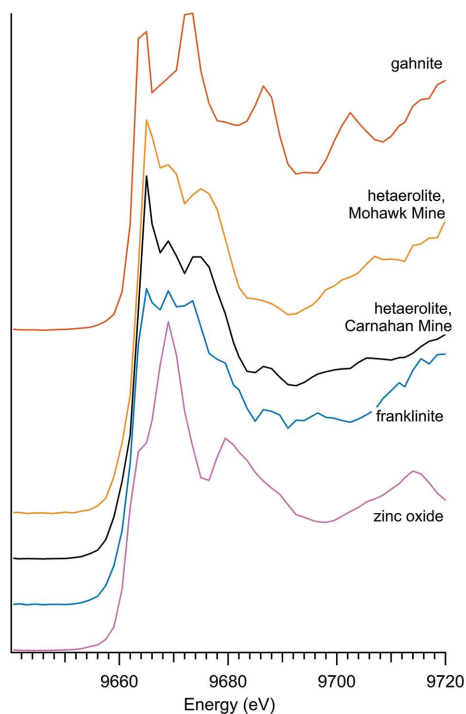


Figure 7
Spectra of zinc oxides.

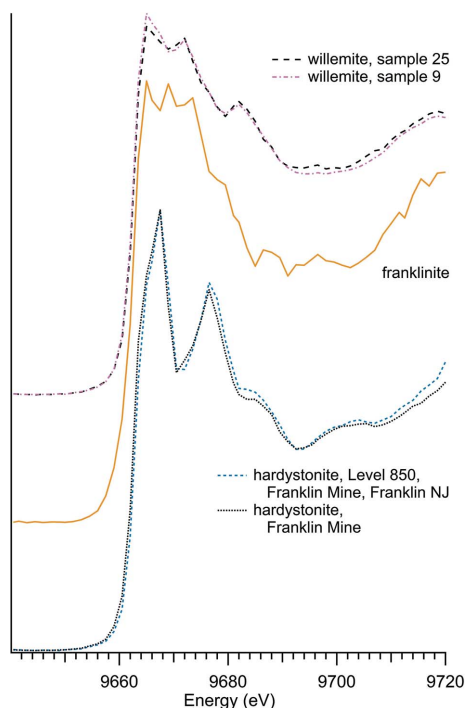


Figure 8
Comparison of franklinite spectra with zinc silicates.

3.6. Organic zinc compounds

The six organic zinc compounds (Table 6) shared a general spectral shape (Fig. 9), with the significant exception of zinc protoporphyrin, but their peak energy varied more than the other subgroups represented here. For zinc acetate and zinc stearate, the energy peak was shifted to 9665 eV, as illustrated in Table 6. The organic zinc

samples had a wide main peak, which is most readily observed with the carbonic anhydrase.

The peaks around the *K*-edge of zinc protoporphyrin were closely aligned across all four synchrotron runs; however, the position and intensity of subtle peaks at energies above the *K*-edge were somewhat variable between synchrotron runs for this material.

3.7. Additional zinc compounds

Other zinc compounds, which did not fit into the previous categories, include zinc halogens and zinc sulfides (Table 7). There were three samples which contained zinc and sulfur, shown in Fig. 10, and two halogen samples, which included zinc bromide and zinc chloride, illustrated in Fig. 11.

Sphalerite has a strong edge and closely aligned peak, but the sphalerite samples were consistently noisy on the post-edge, past about 5 eV from the *K*-edge peak energy. While the presence of iron, visually apparent through the black color of the sphalerite (Hurlbut, 1941), could impact the spectral shape, both sphalerite samples were almost colorless, indicating a very low iron content. This assessment is further

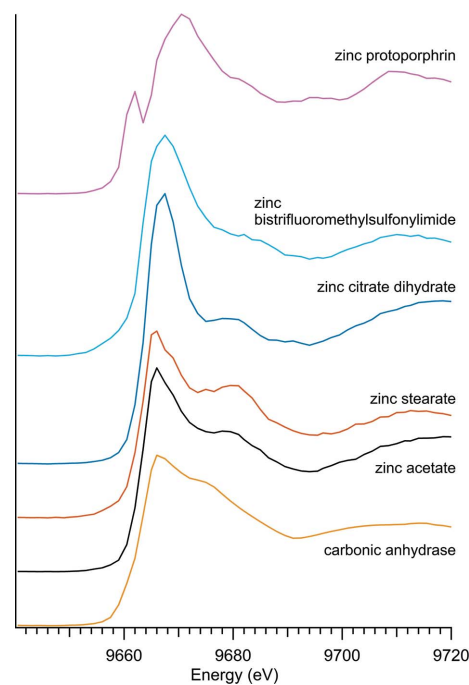


Figure 9
Spectra of organic zinc.

Table 6
Organic zinc samples.

Sample number	Name	Ideal chemical formula	Locality	E_0 (eV)
N/A	Carbonic anhydrase		MP Biomedicals 153879	9665.0
10	Zinc acetate	$Zn(CH_3COO)_2 \cdot 2H_2O$	EM CAS5970-45-6	9665.0
20	Zinc bis (trifluoromethylsulfonyl)imide	$C_4F_{12}N_2O_8S_4Zn$	Alfa Aesar (chemical formula from #46880)	9663.5
14	Zinc citrate dihydrate	$(C_6H_5O_7)_2Zn_3 \cdot 2H_2O$	Aldrich 480762	9663.5
N/A	Zinc protoporphyrin, 96%	$C_{34}H_{32}N_4O_4Zn$	Alfa Aesar	9660.5
18	Zinc stearate	$C_{36}H_{70}O_4Zn$	Alfa 33238	9665.0

Table 7
Additional zinc compounds.

Sample number	Name	Ideal chemical formula	Locality	E_0 (eV)
7	Sphalerite	ZnS	Private collection, unknown location	9662.0
27	Sphalerite	ZnS	Private collection, unknown location	9662.0
11	Zinc bromide	$ZnBr_2$	Acros A0356300	9664.0
13	Zinc chloride	$ZnCl_2$	Alfa A16281	9665.0
23	Zinc sulfide	ZnS	Alfa Aesar 40091	9662.0

informed by observing the spectra of sphalerite, which is closely matched to the synthetic zinc sulfide.

Both zinc bromide and zinc chloride exhibited a strong peak and a nearly featureless post-edge.

4. Conclusions

The consistency of spectral patterns between specimens of the same mineral from different localities suggests that natural compositional variations will not influence identification of these phases in unknown samples. The variety of distinctive

spectra features for the minerals, compounds and organic species will aid in the identification of pure forms of these species and will also be helpful in the application of spectral linear combination approaches for the identification of unknowns in mixtures.

Acknowledgements

The data used to establish these results is available in the supplementary materials. Any opinions, findings, and conclusions or recommendations expressed in this material are those of the authors and do not necessarily reflect the views of the National Science Foundation.

Funding information

The following funding is acknowledged: National Science Foundation, Division of Ocean Sciences (grant No. 1357375; grant No. 1658181; grant No. 1658311 to Peter L. Morton); US Department of Energy (contract No. DE-AC02-06CH11357 to

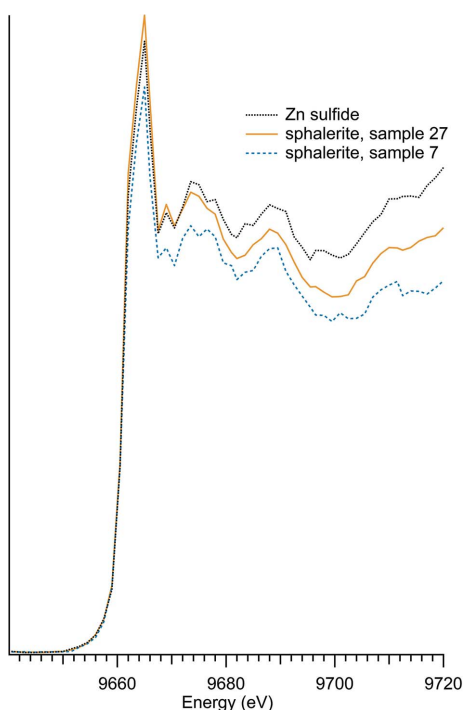


Figure 10
Zinc sulfur spectra.

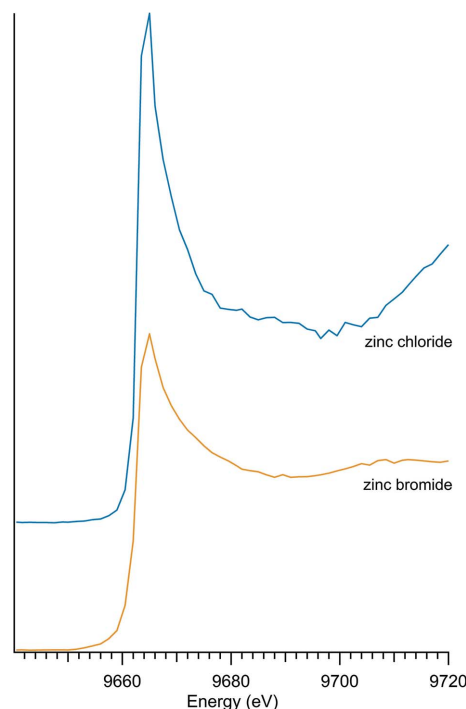


Figure 11
Zinc halogen spectra.

Barry Lai, Advanced Photon Source at Argonne National Laboratory); National Science Foundation, Division of Electrical, Communications and Cyber Systems (grant No. 1542174 to Georgia Tech Institute for Electronics and Nanotechnology).

References

- Abe, H., Aquilanti, G., Boada, R., Bunker, B., Glatzel, P., Nachttegaal, M. & Pascarelli, S. (2018). *J. Synchrotron Rad.* **25**, 972–980.
- Adediran, G. A., Ngwenya, B. T., Mosselmans, J. F. W., Heal, K. V. & Harvie, B. A. (2015). *J. Hazard. Mater.* **283**, 490–499.
- Bazin, D., Carpentier, X., Brocheriou, I., Dorfmueller, P., Aubert, S., Chappard, C., Thiaudière, D., Reguer, S., Waychunas, G., Jungers, P. & Daudon, M. (2009). *Biochimie*, **91**, 1294–1300.
- Cheng, M., Kopittke, P. M., Wang, A., Sale, P. W. G. & Tang, C. (2018). *Plant Soil*, **430**, 219–231.
- Da Silva-Cadoux, C., Zanella, L. & Gaillard, J.-F. (2012). *J. Anal. At. Spectrom.* **27**, 957–965.
- Dessombz, A., Nguyen, C., Ea, H.-K., Rouzière, S., Foy, E., Hannouche, D., Réguer, S., Picca, F.-E., Thiaudière, D., Lioté, F., Daudon, M. & Bazin, D. (2013). *J. Trace Elem. Med. Biol.* **27**, 326–333.
- Doolette, C. L., Read, T. L., Li, C., Scheckel, K. G., Donner, E., Kopittke, P. M., Schjoerring, J. K. & Lombi, E. (2018). *J. Exp. Bot.* **69**, 4469–4481.
- Ellwood, M. J. & Hunter, K. A. (2000). *Limnol. Oceanogr.* **45**, 1517–1524.
- Frenkel, A. I., Hills, C. W. & Nuzzo, R. G. (2001). *J. Phys. Chem. B*, **105**, 12689–12703.
- Gao, J., Zhu, F., Lai, X., Huang, R., Qin, S., Chen, D., Liu, J., Zheng, L. & Wu, X. (2014). *High. Press. Res.* **34**, 89–99.
- Gaur, A., Shrivastava, B. D. & Joshi, S. K. (2009). *J. Phys. Conf. Ser.* **190**, 012084.
- Gervais, C., Thoury, M., Réguer, S., Gueriau, P. & Mass, J. (2015). *Appl. Phys. A*, **121**, 949–955.
- Gräfe, M., Donner, E., Collins, R. N. & Lombi, E. (2014). *Anal. Chim. Acta*, **822**, 1–22.
- Hamilton, J. G., Farrell, R. E., Chen, N., Feng, R., Reid, J. & Peak, D. (2016). *J. Environ. Qual.* **45**, 684–692.
- Hurlbut, C. S. (1941). *Dana's Manual of Mineralogy*, 15th ed. New York: John Wiley & Sons.
- Ingall, E., Feng, Y., Longo, A., Lai, B., Shelley, R., Landing, W., Morton, P., Nenes, A., Mihalopoulos, N., Violaki, K., Gao, Y., Sahai, S. & Castorina, E. (2018). *Atmosphere* **9**, 201.
- Isaure, M. P., Manceau, A., Geoffroy, N., Laboudigue, A., Tamura, N. & Marcus, M. A. (2005). *Geochim. Cosmochim. Acta*, **69**, 1173–1198.
- Jacquat, O., Voegelin, A. & Kretzschmar, R. (2009). *Geochim. Cosmochim. Acta*, **73**, 5256–5272.
- Leinweber, P., Kruse, J., Walley, F. L., Gillespie, A., Eckhardt, K.-U., Blyth, R. & Regier, T. (2007). *J. Synchrotron Rad.* **14**, 500–511.
- Le Pape, P., Quantin, C., Morin, G., Jouvin, D., Kieffer, I., Proux, O., Ghanbaja, J. & Ayraut, S. (2014). *Environ. Sci. Technol.* **48**, 11901–11909.
- Longo, A. F., Ingall, E. D., Diaz, J. M., Oakes, M., King, L. E., Nenes, A., Mihalopoulos, N., Violaki, K., Avila, A., Benitez-Nelson, C. R., Brandes, J., McNulty, I. & Vine, D. J. (2014). *Geophys. Res. Lett.* **41**, 4043–4049.
- Löscher, B. M. (1999). *Mar. Chem.* **67**, 67–102.
- Malviya, S., Scalco, E., Audic, S., Vincent, F., Veluchamy, A., Poulain, J., Wincker, P., Iudicone, D., de Vargas, C., Bittner, L., Zingone, A. & Bowler, C. (2016). *Proc. Natl Acad. Sci. USA*, **113**, E1516–E1525.
- Mamindy-Pajany, Y., Sayen, S., Mosselmans, J. F. W. & Guillon, E. (2014). *Environ. Sci. Technol.* **48**, 7237–7244.
- Manceau, A., Marcus, M. & Tamura, N. (2002). *Rev. Mineral. Geochem.* **49**, 341–428.
- Monsant, A. C., Kappen, P., Wang, Y., Pigram, P. J., Baker, A. J. M. & Tang, C. (2011). *Plant Soil*, **348**, 167–183.
- Oakes, M., Weber, R. J., Lai, B., Russell, A. & Ingall, E. D. (2012). *Atmos. Chem. Phys.* **12**, 745–756.
- Ravel, B. & Newville, M. (2005). *J. Synchrotron Rad.* **12**, 537–541.
- Rivera, N., Hesterberg, D., Kaur, N. & Duckworth, O. W. (2017). *Energy Fuels*, **31**, 9652–9659.
- Rouff, A. A., Eaton, T. T. & Lanzirrotti, A. (2013). *Chemosphere*, **93**, 2159–2164.
- Sarret, G., Balesdent, J., Bouziri, L., Garnier, J.-M., Marcus, M. A., Geoffroy, N., Panfili, F. & Manceau, A. (2004). *Environ. Sci. Technol.* **38**, 2792–2801.
- Sunda, W. G. & Huntsman, S. A. (2005). *Limnol. Oceanogr.* **50**, 1181–1192.
- Tella, M., Bravin, M. N., Thuriès, L., Cazeveille, P., Chevassus-Rosset, C., Collin, B., Chaurand, P., Legros, S. & Doelsch, E. (2016). *Environ. Pollut.* **212**, 299–306.
- Wang, L., Lu, X. & Huang, Y. (2013). *X-ray Spectrom.* **42**, 423–428.
- Wang, Y., Li, A., Zhan, Y., Wei, L., Li, Y., Zhang, G., Xie, Y., Zhang, J., Zhang, Y. & Shan, Z. (2007). *J. Radioanal. Nucl. Chem.* **273**, 247–251.
- Waychunas, G. A., Fuller, C. C., Davis, J. A. & Rehr, J. J. (2003). *Geochim. Cosmochim. Acta*, **67**, 1031–1043.
- Webb, S. & Gaillard, J.-F. (2015). *Aquat. Geochem.* **21**, 295–312.
- Yamamoto, K. & Hashimoto, Y. (2017). *J. Environ. Qual.* **46**, 461–465.
- Zhou, D., Jia, H., Rana, J., Placke, T., Scherb, T., Kloepsch, R., Schumacher, G., Winter, M. & Banhart, J. (2017). *Electrochim. Acta*, **246**, 699–706.